Available online at www.sciencedirect.com
ScienceDirect
Journal of Computational Physics 218 (2006) 82–101
JOURNAL OF COMPUTATIONAL PHYSICS
www.elsevier.com/locate/jcp

A family of time-staggered schemes for integrating hybrid DPD models for polymers: Algorithms and applications

Vasileios Symeonidis, George Em Karniadakis *

Division of Applied Mathematics, Brown University, 182 George Street, Box F, Providence, RI 02912, USA

Received 15 August 2005; received in revised form 23 January 2006; accepted 27 January 2006
Available online 15 March 2006

Abstract

We propose new schemes for integrating the stochastic differential equations of dissipative particle dynamics (DPD) in simulations of dilute polymer solutions. The hybrid DPD models consist of hard potentials that describe the microscopic dynamics of polymers and soft potentials that describe the mesoscopic dynamics of the solvent. In particular, we develop extensions to the velocity-Verlet and Lowe's approaches – two representative DPD time-integrators – following a subcycling procedure whereby the solvent is advanced with a timestep much larger than the one employed in the polymer time-integration. The introduction of relaxation parameters allows optimization studies for accuracy while maintaining the low computational complexity of standard DPD algorithms. We demonstrate through equilibrium simulations that a 10-fold gain in efficiency can be obtained with the time-staggered algorithms without loss of accuracy compared to the non-staggered schemes. We then apply the new approach to investigate the scaling response of polymers in equilibrium as well as the dynamics of λ-phage DNA molecules subjected to shear.

Keywords: Multi-scale modeling; Non-Newtonian fluids; DNA; Hard potentials

1. Introduction

In many systems of soft condensed matter there is often a disparity in time and length scales between the various components of the system. In simulating polymers, in particular, the primary aim is to investigate the scaling response of the system without paying much attention to the underlying chemistry. Moreover, the spatiotemporal dynamics for the polymer chains and for the solvent may be substantially different. In highly concentrated polymer solutions the hydrodynamic forces due to solvent do not significantly affect the dynamical properties of the system. However, in dilute polymer solutions the solvent hydrodynamics plays an important role, possibly causing long-ranged interactions between different parts of the polymer chain [1].

The standard molecular dynamics (MD) method is not effective in simulating such systems due to the inherent time step limitation of about 10^{-15} s and the fact that most of the available CPU is typically spent

* Corresponding author. Tel.: +1 401 863 1217; fax: +1 401 863 3369.
E-mail address: gk@dam.brown.edu (G.E. Karniadakis).

0021-9991/$ - see front matter
doi:10.1016/j.jcp.2006.01.043

in propagating solvent molecules. In order to efficiently simulate this *multirate dynamics* of dilute polymer solutions, several *hybrid* numerical models have been developed in recent years that treat separately the solvent and the polymer. In the hybrid approach the polymer chains are described at a molecular level by hard interactions whereas the solvent can be described on a simpler level in terms of soft pair potentials or some other simplified hydrodynamic description. To this end, the authors of [2] combined a lattice Boltzmann method (LBM) with a continuum molecular dynamics (MD) model for the polymer chain to simulate polymer–solvent systems. They found that the combined LBM-MD approach achieves a speed-up factor of 20 compared to a pure MD for comparable accuracy in the results. Similarly, in [3–5] Malevanets and collaborators introduced a hybrid model consisting of a direct simulation Monte Carlo (DSMC) algorithm for the solvent and MD for the polymer chain and found good agreement with semi-analytical benchmark results. The proposed method (called *multiparticle collision dynamics* or *stochastic rotation dynamics*) was further used in [6] for two-dimensional polymer chains in good solvent conditions and the dynamical scaling was verified. Furthermore, in [7] the same technique was used for the study of vesicles under shear.

Dissipative particle dynamics (DPD) is a mesoscopic numerical method introduced in [8], while the studies in [9] defined the DPD model and allowed applications to emerge. The technique was first employed for simulating dilute polymer solutions in [10]. The solvent particles represent clusters of actual atoms that interact pairwise via simple soft potentials. The polymer beads are also represented by particles subject to standard DPD forces but in addition they exchange momentum with their neighbors according to an elastic spring force and through other repulsive forces corresponding to hard potentials [11]. In their original work in [10] the authors report a speed-up factor of 60 compared to the MD simulations reported in [12]. Since that work, however, several papers have appeared in the literature that present effective time integrators for DPD for single-phase systems as well as for solvent–polymer systems [11,13–18]. A systematic evaluation of these time-integrators (with the exception of the new scheme in [17]) was presented in [19] where a hybrid model for polymers was also investigated, while the authors of [18] presented four variants of the popular velocity-Verlet algorithm. In DPD simulations the results are timestep dependent for large values of the timestep but some models, such as Lowe's scheme [15] (also the scheme in [17]), perform much better than others. A specific result of interest to the current work reported in [19] is that for the hybrid solvent–polymer system involving soft–hard potentials the maximum timestep for good accuracy is a factor of 20 smaller than the timestep for simulating the solvent-only. For example, employing Lowe's approach, the maximum timestep for the hybrid system was $\Delta t_{\mathrm{h}} \approx 0.02$ whereas for the solvent-only it was $\Delta t_{\mathrm{s}} \approx 0.4$. Accuracy here is measured by deviations of the observed kinetic temperature $\langle k_{\mathrm{B}} T \rangle$ from the imposed equilibrium temperature of the system. Moreover, deviations in the polymer chain temperature dominate the deviations in the temperature of the *entire* solvent–polymer system even for the dilute system they examined with more than 99.5% of the DPD particles being solvent particles.

These findings suggest that the hybrid model can be further enhanced if the multirate dynamics of the polymer and solvent are treated separately, i.e., using different timesteps δt and Δt, respectively, to integrate the DPD governing equations. To this end, in this work we develop a staggered scheme, similar to the subcycling technique used in classical computational fluid dynamics (CFD) time-integration methods (e.g., semi-Lagrangian method in advection–diffusion systems, see [20]). In particular, for the DPD equations we will integrate the solvent (soft potential) with a large timestep Δt while we will perform several substeps for the polymer (hard potential). A similar approach was used in an earlier work [21] for multiple-timestep MD Verlet-type integrators. In order to evaluate this approach, we consider two representative time-integrators: the DPD velocity-Verlet algorithm (vV) [22,11,19] which integrates the standard DPD equations, and also Lowe's algorithm which provides an alternative approach [15]. We have to note that although the latter does not discretizate the DPD equations, the modified approach presented in [17] does.

A typical system we will consider in this work is shown in Fig. 1; it consists of a few chains (large particles) representing the polymer beads and smaller particles representing the solvent. A sketch of the corresponding potentials that govern this system is shown in Fig. 2. The standard time-integrators employed in MD simulations are not applicable to this system due to the random and dissipative forces, in addition to the conservative forces, present in the equations of motion. In particular, the dissipative forces depend on the velocity and this makes the equations of motion nonlinear. This, in turn, implies that a sub-iteration should be employed in order to produce a consistent time-integration scheme otherwise numerical artifacts are produced

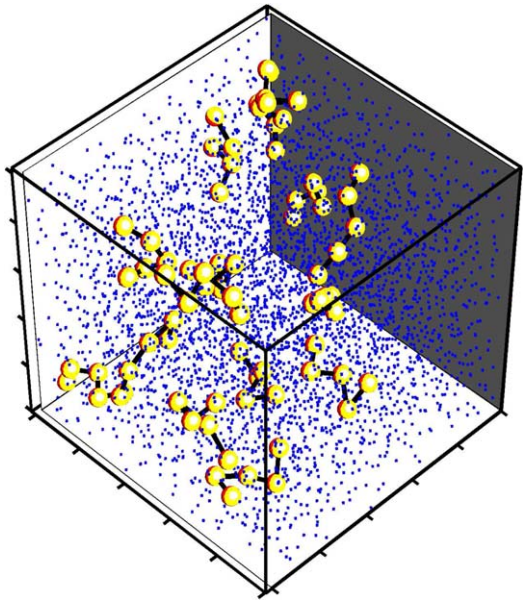

Fig. 1. Polymer chains (tethered spheres) suspended in a solvent of DPD particles (smaller dots).

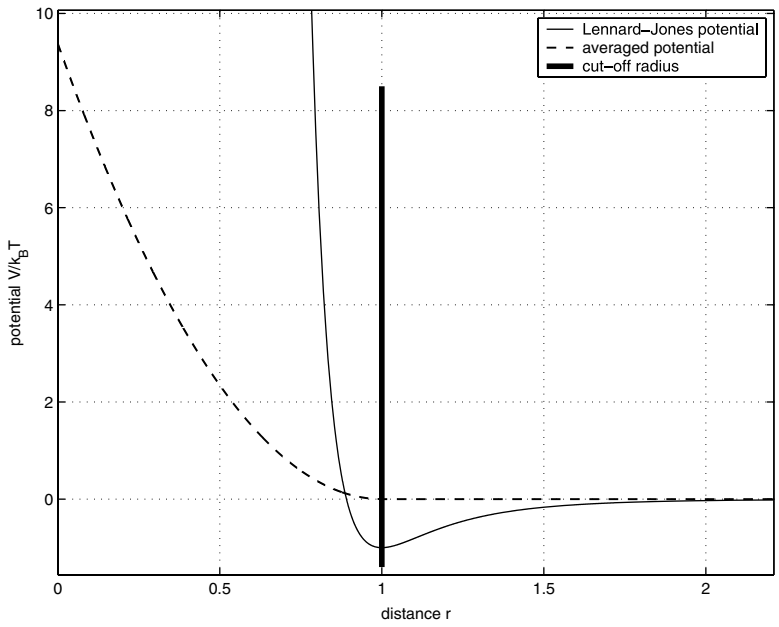

Fig. 2. Lennard-Jones potential and the soft-repulsive potential which results after averaging.

[13,19,23]. This problem is especially pronounced in the absence of conservative forces, e.g. in simulating the so-called dissipative gas. Here, we model the solvent as *liquid* throughout the work, so we will make use of a modified velocity-Verlet algorithm (vV) proposed by Groot and Warren that does not include a sub-iteration. Instead, it introduces a relaxation parameter, λ, which is used to minimize integration errors in the DPD system.

Motivated by the success of Groot and Warren's approach, we introduce in the present work a family of new relaxation parameters in various sub-steps involving predicting–correcting action in the time-integration of the polymer–solvent system. We then perform systematic numerical simulations of the system shown in

Fig. 1 at equilibrium conditions in order to determine the best values of the relaxation parameters. After completion of such accuracy tests, we apply the new staggered algorithms in order to quantify the scaling of the radius of gyration of flexible polymer chains described by different polymer models and hard potentials. We also investigate the accuracy and robustness of the new time-integrators in simulating the response of λ-phage DNA molecules under shear, and we compare our findings with available experimental results.

The paper is organized as follows: in Section 2, we summarize the standard governing equations, and in Section 3 we give an overview of the polymer models that we will employ. In Section 4, we present the standard and staggered time-integrators based on the velocity-Verlet and Lowe's schemes. In Section 5, we present the various simulation tests we performed and obtain a set of optimum values for the relaxation parameters we introduced in the two time-integration schemes. In Section 6, we present results of the computational complexity of the method. In Sections 7 and 8, we show results from the two aforementioned applications, and we conclude in Section 9 with a brief summary.

2. The DPD equations

We consider a system of N particles, each having mass m_i, whose momenta and position vectors are governed by Newton's equations of motions. In particular, for a typical particle i

$$\mathbf{v}_i = \dot{\mathbf{r}}_i, \tag{1a}$$

$$\mathbf{F}_i = m_i \dot{\mathbf{v}}_i, \tag{1b}$$

where $\mathrm{d}/\mathrm{d}t$ is denoted by overdot, $\mathbf{v}_i$ is the particle velocity, $\mathbf{r}_i$ its position vector and $\mathbf{F}_i$ the net force. Throughout this work we choose $m_i = 1$. The interparticle force $\mathbf{F}_{ij}$ exerted on particle i by particle j is composed of conservative ($\mathbf{F}^{\mathrm{c}}_{ij}$), dissipative ($\mathbf{F}^{\mathrm{d}}_{ij}$) and random ($\mathbf{F}^{\mathrm{r}}_{ij}$) components. Hence the total force on particle i is given by

$$\mathbf{F}_i = \sum_{i \neq j} \mathbf{F}^{\mathrm{c}}_{ij} + \mathbf{F}^{\mathrm{d}}_{ij} + \mathbf{F}^{\mathrm{r}}_{ij}. \tag{2}$$

The above sum acts over all particles within a cutoff radius r_{c} above which the forces are considered negligible. This interaction radius is set to $r_{\mathrm{c}} = 1$ and defines the length scale of the system. Denoting $\mathbf{r}_{ij} = \mathbf{r}_i - \mathbf{r}_j$, $\mathbf{v}_{ij} = \mathbf{v}_i - \mathbf{v}_j$, $r_{ij} = |\mathbf{r}_{ij}|$ and the unit vector $\mathbf{e}_{ij} = \frac{\mathbf{r}_{ij}}{r_{ij}}$ we further define each of the forces to take the following form:

$$\mathbf{F}^{\mathrm{c}}_{ij} = F^{(c)}(r_{ij})\mathbf{e}_{ij}, \tag{3a}$$

$$\mathbf{F}^{\mathrm{d}}_{ij} = -\gamma \omega^{\mathrm{d}}(r_{ij})(\mathbf{v}_{ij} \cdot \mathbf{e}_{ij})\mathbf{e}_{ij}, \tag{3b}$$

$$\mathbf{F}^{\mathrm{r}}_{ij} = \sigma \omega^{\mathrm{r}}(r_{ij})\xi_{ij}\mathbf{e}_{ij}, \tag{3c}$$

where ξ_{ij} are symmetric Gaussian random variables with zero mean and unit variance and σ, γ are *not* independent, as shown below. Newton's equations of motions govern each particle's motion through

$$\mathrm{d}\mathbf{r}_i = \mathbf{v}_i \delta t, \tag{4a}$$

$$\mathrm{d}\mathbf{v}_i = \frac{\mathbf{F}^{\mathrm{c}}_i \delta t + \mathbf{F}^{\mathrm{d}}_i \delta t + \mathbf{F}^{\mathrm{r}}_i \sqrt{\delta t}}{m_i}, \tag{4b}$$

where the factor $\sqrt{\delta t}$ appears because the random forces are interpreted as Wiener processes.

The conservative force $\mathbf{F}^{\mathrm{c}}_{ij}$ is similar to that in the MD formulation. It can be any force derivable from a predefined potential and can be tailored to each individual simulation problem. Possible choices include electrostatic forces, spring-type (Hookean, FENE), van der Waals, hard repulsions (Lennard-Jones) or soft repulsions (potential pre-averaged forces in the spirit of [24]). Hence, $\mathbf{F}^{\mathrm{c}}_{ij}$ is not constrained or defined by the DPD equations. This force as well as the other two act within a sphere of radius r_{c}, which defines the length scale of the system; it corresponds to a *soft repulsive-only* interaction potential. By averaging the Lennard-Jones potentials or the corresponding molecular field over the *rapidly* fluctuating motions of atoms over short time intervals, an effective average potential is obtained of the form shown in Fig. 2. A linear approximation of this is as follows [11]:

$$F^{(c)}(r_{ij}) = \begin{cases} a_{ij}(1 - \frac{r_{ij}}{r_c}) & \text{if } r_{ij} \leqslant r_c, \\ 0 & \text{if } r_{ij} > r_c. \end{cases} \tag{5}$$

Unlike the hard Lennard-Jones potential which is unbounded at $r = 0$, the *soft potential* employed in DPD has a finite value a_{ij} at $r = 0$. The dissipative and random forces, on the other hand, are characterized by strengths $\omega^d(r_{ij})$ and $\omega^r(r_{ij})$ coupled by the *fluctuation–dissipation* relations [9]

$$\omega^d(r_{ij}) = [\omega^r(r_{ij})]^2 = \begin{cases} \left(1 - \frac{r_{ij}}{r_c}\right)^2 & \text{if } r_{ij} \leqslant r_c, \\ 0 & \text{if } r_{ij} > r_c, \end{cases} \tag{6a}$$

$$\sigma^2 = 2\gamma k_B T. \tag{6b}$$

3. Models for polymers

Unlike the MD equations, the DPD equations are stochastic and nonlinear since the dissipative force depends on the velocity. In particular, for complex fluids the presence of both soft and hard potentials suggests the use of time-staggered algorithms for integrating the DPD equations of motion. This allows the efficient study of polymeric physical quantities, such as the radius of gyration of the polymeric chain. The conservative forces present in the usual DPD equations can be tailored in such a way so as to describe a variety of interactions, e.g., Lennard-Jones (LJ), Hookean dumbells, Finitely extensible nonlinear elastic (FENE) springs and van der Waals forces – as long as they are derivable from a given potential $V(r_{ij})$. Fig. 2 illustrates the need for two different temporal resolutions: the Lennard-Jones (LJ) potential (for bead–bead pairs) is a hard repulsion that requires a timestep much smaller than the soft interaction forces of a typical DPD particle pair, which can be thought of as an *averaged* soft potential.

The polymeric chains consist of beads (DPD particles) subject to the standard DPD forces: soft repulsive (conservative), dissipative and random. *In addition* to these forces, they are subject to intra-polymer forces, arising from different combinations of the following types:

- *Lennard-Jones repulsion*. The repulsion for each pair of bead particles is given by the shifted LJ potential

  $$U_{LJ} = 4\epsilon\left[\left(\frac{L}{r_{ij}}\right)^{12} - \left(\frac{L}{r_{ij}}\right)^{6} + \frac{1}{4}\right]$$

  truncated to act *only* for pairs with $r_{ij} < r_c$. We set $\epsilon = k_B T$, $L = 2^{-1/6}$ and $r_c = L \times 2^{-1/6} = 1$. We note that the LJ potential used here is defined at the mesoscopic level to improve polymeric self-avoidance; softer repulsion rules are an alternative approach [25].
- *FENE spring*. Within a chain of M beads each bead is subject to a pairwise nonlinear spring force. The finitely extensible nonlinear elastic (FENE) spring has a maximum extensibility r_{max} beyond which the force becomes infinite, and hence any length greater than r_{max} is considered unphysical and is not allowed. The potential is described by

  $$U_{FENE} = -\frac{\kappa}{2} r_{max}^2 \log\left[1 - \frac{|\vec{r}_i - \vec{r}_{i-1}|^2}{r_{max}^2}\right], \quad \text{where } i = 2, 3, 4, \ldots, M$$

  and κ the spring constant.
- *Marko–Siggia worm-like chain*. Polymer models of biological importance (DNA, proteins) have been known to be governed by stiff interactions. The worm-like chain [26–28] can be thought of as a continuous curve in three-dimensional space. Of importance is the *persistence length* λ_p, which is a measure of the chain's stiffness and is the average length over which the orientation of a curve segment does not change (''persists''). We will focus on the bead-spring representation of the model, which approximates a portion of the worm-like chain with a force law given by the Marko–Siggia [29] expression

$$F^{(c)} = \frac{k_B T}{\lambda_p}\left[\frac{1}{4(1-R)^2} - \frac{1}{4} + R\right], \quad \text{where } R = \frac{|\vec{r}_i - \vec{r}_{i-1}|}{L_{\text{spring}}} = \frac{r}{L_{\text{spring}}} \quad i = 2, 3, 4, \ldots, M$$

and L_{spring} is the maximum allowed length for each chain (spring) segment. The expression is accurate for large values of the ratio $\frac{L_{\text{spring}}}{\lambda_p}$ and exact as $r \to 0$ or $r \to L_{\text{spring}}$.

The inter-bead force in each case is $\mathbf{F}^p = -\nabla U$. Note that the bonded interactions (spring forces) are pairwise but act only between consecutive beads in a chain (i.e., bead number i exerts spring forces on beads $i-1$, $i+1$) only, whereas the non-bonded interactions, like the repulsive LJ force, act in a pairwise fashion that depends on the instantaneous relative position of the beads. This fundamental difference requires neighbor-search routines for the latter.

The Marko–Siggia spring law is an averaged quantity, locally approximating flexible rods. The derivation of the formula accounts for coarse-graining microscopic elements of a long chain (such as bead-rod), by use of statistical mechanics. However, in order to use the Marko–Siggia law in molecules with more than two beads (dumbbells), some authors [30] account for the different stiffness of the beaded counterparts by altering the persistence length λ_p of the sub-chains. Detailed analysis of such arguments [31] has shown that it is possible to minimize the errors arising by the introduction of beads and sub-chains. Throughout this work we will adopt the analysis presented in [31] for stained λ-phage DNA molecules assumed to have $L = 21.1$ μm (fully extended length) and $\lambda_p = 0.053$ μm (persistence length). The correction we will apply will linearly approximate the ratio of effective to true persistence length, for three different regions of the extension: low force, half-extended spring and high-force regimes. More specifically, we define the ratio

$$\lambda^\star = \frac{\lambda_p[\text{EFFECTIVE}]}{\lambda_p[\text{TRUE}]}$$

so that when $\lambda^\star = 1$ no correction is applied. The tables in [31] suggest a high, medium and zero correction for the low-force, half-extension and high-force regions, respectively. We go one step further to introduce a linear fit to the suggested correction values for M-bead chains:

$$\lambda^\star \approx (1.0 - \hat{z}) \times 0.022 \times (M-1) + 1 \quad \text{if } M \leqslant 20,$$
$$\lambda^\star \approx (1.0 - \hat{z}) \times 0.025 \times (M-1) + 1 \quad \text{if } M > 20,$$

where $0 \leqslant \hat{z} \leqslant 1$ is the instantaneous fractional extension of the whole molecule in the stretching direction. The above expressions approximate fairly accurately the values given in [31] and are implemented in all instances of $M > 2$ for the Marko–Siggia spring force in this work.

In summary, the solvent beads are described by soft DPD interactions only (conservative, dissipative and random) while intra-molecular interactions between polymer beads include these DPD-type forces but also combinations of the above bonded and non-bonded interactions.

4. Time-staggered schemes

The two basic DPD integrating schemes we will consider in this work are: a modified version of the classical velocity-Verlet algorithm (vV) – as outlined by Groot and Warren [11] – and Lowe's algorithm [15,19]. The vV scheme is characterized by explicit calculation of all forces $\mathbf{F}^c$, $\mathbf{F}^d$, $\mathbf{F}^r$ (conservative, dissipative and random) and is known to be timestep dependent, but at the same time straightforward and relatively accurate. Lowe's method, on the other hand, is a scheme similar to the Andersen thermostat [32] with the particle velocities corrected every timestep using the Maxwell velocity distribution. In absence of conservative forces, which are integrated in the vV manner, the scheme is shown to be independent of the chosen timestep Δt [19], although a recent work [23] has shown that the scheme can give rise to some minor artifacts. The core operation in Lowe's method involves re-equilibration of the particle momenta at one step with an updated inter-particle relative velocity drawn from a Gaussian distribution.

4.1. Time-staggered velocity-Verlet scheme

The vV DPD scheme relies on a basic predictor–corrector approach, which uses provisional values of the velocities for the force calculations, which are corrected at the end of each timestep. It is important to keep in mind that the DPD dissipative forces depend on the relative velocities of the particles, hence this prediction is crucial. Below we outline the modified vV scheme with parameter λ. The theoretical value is $\lambda = 0.5$ but Groot and Warren [11] have shown empirically that for a certain range of Δt the optimal value is closer to $\lambda = 0.65$ when $k_B T = 1$. In this work all results presented use the latter, since our timestep is in the optimal range of $\mathcal{O}(10^{-2})$. In the following discussion, we denote the total forces by $\mathbf{F}_i = \sum_{j\neq i}\left[\mathbf{F}^{\mathrm{c}}_{ij} + \mathbf{F}^{\mathrm{d}}_{ij} + \frac{\mathbf{F}^{\mathrm{r}}_{ij}}{\sqrt{\Delta t}}\right]$ and the extra polymeric forces by $\mathbf{F}^{\mathrm{p}}_i = \sum_{j\neq i}\mathbf{F}^{\mathrm{p}}_{ij}$.

To extend this algorithm for the simulation of complex fluids with soft/hard potentials, a large timestep, Δt, is employed for solvent particles and a smaller one, δt, for polymer particles belonging to a chain. To this end, we use provisional values not only for the velocity of the solvent and the polymer, but also the position of the polymer. The CPU-expensive step of collective force computation is done only once. The velocity *and* the position of the polymer are corrected in the subsequent loop, in which we integrate the polymer particles $\mathbb{K} = \frac{\Delta t}{\delta t}$ times in a separate subcycle (using δt for the timestep). The varying polymeric force $\mathbf{F}^{\mathrm{p}}_i$ is updated within the subcycle, following the change in $\mathbf{r}_{p_i}$, the position of the polymer particles. Hence, during the subcycle we update the intra-polymer forces, but not the inter-particle (total) ones. This would require CPU time for each subcycle equivalent to a standard one. Although we cannot expect exact agreement of the new scheme with the classical one, we can anticipate small differences if the ratio $\frac{\Delta t}{\delta t}$ is not too large and if the (outdated) forces are applied in the correct manner during the δt cycle. The algorithm is summarized in Table 1. The proposed scheme depends on the relaxation parameters μ, α, β and λ and the subscripts 'p', 's' correspond to polymer and solvent quantities, respectively. It has to be noted that multiple timestep algorithms may be subject to resonance, which may significantly limit the longest timestep [21,33]. In the following section, we will investigate numerically the optimum values for these parameters.

Table 1
Overview of the time-staggered velocity-Verlet approach for a polymer system

$\mathbb{K} = \frac{\Delta t}{\delta t}$, μ, α, β, λ: relaxation parameters	
▶ $\mathbf{r}_{s_i} \leftarrow \mathbf{r}_{s_i} + (\Delta t)\mathbf{u}_{s_i} + \frac{(\Delta t)^2}{2m}\mathbf{F}_i$	Solvent
▶ $\hat{\mathbf{r}}_{p_i} \leftarrow \mathbf{r}_{p_i} + (\Delta t)\mathbf{u}_{p_i} + \frac{(\Delta t)^2}{2m}(\mathbf{F}_i + \mathbf{F}^{\mathrm{p}}_i)$	Polymer
▷ $\hat{\hat{\mathbf{r}}}_{p_i} \leftarrow \mu\mathbf{r}_{p_i} + (1-\mu)\hat{\mathbf{r}}_{p_i}$	Polymer
▶ $\hat{\mathbf{u}}_{s_i} \leftarrow \mathbf{u}_{s_i} + \lambda(\Delta t)\mathbf{F}_i$	Solvent
▶ $\hat{\mathbf{u}}_{p_i} \leftarrow \mathbf{u}_{p_i} + \lambda(\Delta t)(\mathbf{F}_i + \mathbf{F}^{\mathrm{p}}_i)$	Polymer
▷ $\hat{\hat{\mathbf{u}}}_{p_i} \leftarrow \alpha\mathbf{u}_{p_i} + (1-\alpha)\hat{\mathbf{u}}_{p_i}$	Polymer
▶ $\forall_{(i,j)}\quad \widehat{\mathbf{F}}_i \left(\begin{array}{c\|c} \mathbf{r}_s & \hat{\mathbf{u}}_s \\ \hat{\hat{\mathbf{r}}}_{p_i} & \hat{\hat{\mathbf{u}}}_{p_i} \end{array}\right)$	Solvent, polymer
▷ $\hat{\hat{\mathbf{F}}}_i \leftarrow \beta\mathbf{F}_i + (1-\beta)\hat{\mathbf{F}}_i$	Polymer
for $k = 0, 1, \ldots, \mathbb{K}-1$	
$\mathbf{r}_{p_i} \leftarrow \mathbf{r}_{p_i} + (\delta t)\mathbf{u}_{p_i} + \frac{(\delta t)^2}{2m}(\hat{\hat{\mathbf{F}}}_i + \mathbf{F}^{\mathrm{p}}_i)$	Polymer
$\forall_{(i,j)}\mathbf{F}^{\mathrm{p}}_{\dagger_i}(\mathbf{r}_p)$	
$\mathbf{F}_{\mathrm{old}} = \frac{\mathbb{K}-k}{\mathbb{K}}\mathbf{F}_i + \frac{k}{\mathbb{K}}\widehat{\mathbf{F}}_i$	
$\mathbf{F}_{\mathrm{new}} = \frac{\mathbb{K}-(k+1)}{\mathbb{K}}\mathbf{F}_i + \frac{k+1}{\mathbb{K}}\widehat{\mathbf{F}}_i$	
$\mathbf{u}_{p_i} \leftarrow \mathbf{u}_{p_i} + \frac{\delta t}{2}[(\mathbf{F}_{\mathrm{old}} + \mathbf{F}^{\mathrm{p}}_i) + (\mathbf{F}_{\mathrm{new}} + \mathbf{F}^{\mathrm{p}}_{\dagger_i})]$	
$\mathbf{F}^{\mathrm{p}_i} \leftarrow \mathbf{F}^{\mathrm{p}}_{\dagger_i}$	
▶ $\mathbf{u}_{s_i} \leftarrow \mathbf{u}_{s_i} + \frac{\Delta t}{2m}[\mathbf{F}_i + \hat{\mathbf{F}}_i]$	Solvent
▷ $\mathbf{F}_i \leftarrow \widehat{\mathbf{F}}_i$	Solvent
▷ Analyzer	

Table 2
Overview of the time-staggered Lowe's approach for a polymer system

$\mathbb{K} = \frac{\Delta t}{\delta t}$, μ, β: relaxation parameters, Γ: thermalization parameter	
▶ $\mathbf{r}_{s_i} \leftarrow \mathbf{r}_{s_i} + (\Delta t)\mathbf{u}_{s_i} + \frac{(\Delta t)^2}{2m}\mathbf{F}^{\mathrm{c}}_i$	Solvent
▶ $\hat{\mathbf{r}}_{p_i} \leftarrow \mathbf{r}_{p_i} + (\Delta t)\mathbf{u}_{p_i} + \frac{(\Delta t)^2}{2m}[\mathbf{F}^{\mathrm{c}}_i + \mathbf{F}^{\mathrm{p}}_i]$	Polymer
▷ $\hat{\hat{\mathbf{r}}}_{p_i} \leftarrow \mu\mathbf{r}_{p_i} + (1-\mu)\hat{\mathbf{r}}_{p_i}$	Polymer
▶ $\forall_{(i,j)}\widehat{\mathbf{F}}^{\mathrm{c}}_i\begin{pmatrix}\mathbf{r}_s\\ \hat{\hat{\mathbf{r}}}_p\end{pmatrix}$	Solvent, polymer
▷ $\hat{\hat{\mathbf{F}}}^{\mathrm{c}}_i \leftarrow \beta\mathbf{F}^{\mathrm{c}}_i + (1-\beta)\widehat{\mathbf{F}}^{\mathrm{c}}_i$	Polymer
for $k = 0, 1, \ldots, \mathbb{K}-1$	
$\mathbf{r}_{p_i} \leftarrow \mathbf{r}_{p_i} + (\delta t)\mathbf{u}_{p_i} + \frac{(\delta t)^2}{2m}(\hat{\hat{\mathbf{F}}}^{\mathrm{c}}_i + \mathbf{F}^{\mathrm{p}}_i)$	Polymer
$\forall_{(i,j)}\mathbf{F}^{\mathrm{p}}_{\dagger_i}(\mathbf{r}_p)$	
$\mathbf{F}^{\mathrm{c}}_{\mathrm{old}} = \frac{\mathbb{K}-k}{\mathbb{K}}\mathbf{F}^{\mathrm{c}}_i + \frac{k}{\mathbb{K}}\widehat{\mathbf{F}}^{\mathrm{c}}_i$	
$\mathbf{F}^{\mathrm{c}}_{\mathrm{new}} = \frac{\mathbb{K}-(k+1)}{\mathbb{K}}\mathbf{F}^{\mathrm{c}}_i + \frac{k+1}{\mathbb{K}}\widehat{\mathbf{F}}^{\mathrm{c}}_i$	
$\mathbf{u}_{p_i} \leftarrow \mathbf{u}_{p_i} + \frac{\delta t}{2}[(\mathbf{F}^{\mathrm{c}}_{\mathrm{old}} + \mathbf{F}^{\mathrm{p}}_i) + (\mathbf{F}^{\mathrm{c}}_{\mathrm{new}} + \mathbf{F}^{\mathrm{p}}_{\dagger_i})]$	
$\mathbf{F}^{\mathrm{p}}_i \leftarrow \mathbf{F}^{\mathrm{p}}_{\dagger_i}$	
▶ $\forall N_{\mathrm{p}}$ distinct pairs i, j such that $r_{ij} < r_{\mathrm{c}}$	Solvent, polymer
• Generate a Gaussian ξ_{ij} with $\mu = 0$, $\sigma^2 = 1$	
• Form $\mathbf{u}^{\circ}_{ij} \cdot \mathbf{e}_{ij} = \xi_{ij}\sqrt{\frac{2k_{\mathrm{B}}T}{m}}$	
• Generate a uniform distribution ψ_{N_p}	
• If $\psi_{N_p} < \Gamma \times \Delta t \leqslant 1$:	
$2\boldsymbol{\Delta}_{ij} = \mathbf{e}_{ij}(\mathbf{u}^{\circ}_{ij} - \mathbf{u}_{ij}) \cdot \mathbf{e}_{ij}$	
$\mathbf{u}_i \leftarrow \mathbf{u}_i + \boldsymbol{\Delta}_{ij}$	
$\mathbf{u}_j \leftarrow \mathbf{u}_j - \boldsymbol{\Delta}_{ij}$	
▷ $\mathbf{F}^{\mathrm{c}}_i \leftarrow \widehat{\mathbf{F}}^{\mathrm{c}}_i$	Solvent, polymer
▷ $\mathbf{F}^{\mathrm{p}}_i \leftarrow \widehat{\mathbf{F}}^{\mathrm{p}}_i$	Polymer
▷ Analyzer	

4.2. Time-staggered Lowe's scheme

Introduced in 1999, Lowe's method [15] is characterized by the explicit calculation of $\mathbf{F}^{\mathrm{c}}$ and the subsequent re-equilibration of all the particle velocities through a Maxwell distribution. This is done using the *relative* velocities of the particles. The method conserves momentum and introduces an extra parameter Γ so that in the limiting case of $\Gamma \times \Delta t \approx 1$ thermalization/dissipation occurs every timestep. Peters [17] recently introduced a modification of Lowe's scheme by keeping the centroid velocity of a particle-pair unchanged before and after the re-equilibration. This results in an attractive scheme, still independent of the chosen timestep (as opposed to the Verlet approach) that also discretizes the original DPD equations (Lowe's method does *not*). An overview of the traditional Lowe scheme is given in [19].

The fundamental difference between Lowe's and the vV scheme is that dissipative and random forces are not explictly calculated in the former. This feature poses constraints on the construction of the inner δt subcycle. Therefore, we update the conservative solvent forces $\mathbf{F}^{\mathrm{c}}$ once per cycle and the conservative polymeric forces $\mathbf{F}^{\mathrm{p}}$ in every subcycle, following the vV approach. The thermalization is done *once* at the end of the Δt cycle as shown in Table 2.

5. Accuracy tests

5.1. Metrics and simulation parameters

The accuracy of the methods can be measured by monitoring either the temperature of the thermostat or other physical quantities, specific to the polymer system, e.g. the polymeric radius of gyration, R_{g}, or chain temperature, $\langle k_{\mathrm{B}}T \rangle$ (as proposed in [19]), defined, respectively, as

$$\langle R_g^2 \rangle = \left\langle \frac{1}{M} \sum_{i=1}^{M} (R_i - R_{cm})^2 \right\rangle, \quad \langle k_B T \rangle_{chain} = \frac{m}{3M} \left\langle \sum_{i=1}^{M} \mathbf{u}_i^2 \right\rangle$$

for an M-bead chain. Here, R_i denotes the position of bead "i" and R_{cm} the center-of-mass. The presented schemes depend on μ, α, β, λ and Γ. Setting $\lambda = 0.65$ seems to be an appropriate choice [11] for timesteps $\delta t \approx 0.01$, while using the arbitrary value of $\Gamma = 4.5$ will only affect the convergence rate of Lowe's method and not the accuracy. We adopt the choices outlined in Table 3 for $\mathbf{F}_{old}$ and $\mathbf{F}_{new}$ of Tables 1 and 2 in the kth subcycle.

Clearly, the choice of $\mathbf{F}_{old}$, $\mathbf{F}_{new}$ determines how the subcycle treats the second velocity update. In the non-weighted case, we correct the predictions using static values of the old and newly computed total forces. However, the weighted approach accounts for a linear gradient of them, rendering the "old" and "new" total forces old and new *locally in time* within each subcycle δt.

We consider a 4000-DPD particle fluid in equilibrium in a periodic simulation box of dimensions $L_x = L_y = L_z = 10$, thus fixing the number density $\rho = 4$, with 80 of these DPD particles belonging to four different chains, 20-beads each, subject to additional FENE and LJ forcing. The different parameters of the simulation take the following values: the thermal energy level $k_B T = 1$, the mass of each particle $m = 1$, the cutoff distance $r_c = 1$, Lowe's thermalization parameter $\Gamma = 4.5$, the conservative force amplitude $a_{ij} = \frac{75 k_B T}{\rho}$ for both vV and Lowe's schemes, the random force amplitude $\sigma = 3$ (this fixes the dissipative force amplitude to $\gamma = 4.5$), the FENE parameters $r_{max} = 3r_c$, $\kappa = 7$ and the LJ parameters $\epsilon = k_B T$, $L = 2^{-1/6}$, $r_c = L \times 2^{-1/6} = 1$. We note that the resulting system of polymer forces is relatively stiff, with a timestep $\delta t \approx 0.03$ being close to the upper limit for *stability* of the simulation (if we use a non-staggered integrator).

Table 3
Choices for old and new forces acting on polymer beads

	$\mathbf{F}_{old}$	$\mathbf{F}_{new}$
Non-weighted staggering	$\mathbf{F}_i$	$\hat{\mathbf{F}}_i$
Weighted staggering	$\frac{\mathbb{K}-k}{\mathbb{K}} \mathbf{F}_i + \frac{k}{\mathbb{K}} \hat{\mathbf{F}}_i$	$\frac{\mathbb{K}-(k+1)}{\mathbb{K}} \mathbf{F}_i + \frac{k+1}{\mathbb{K}} \hat{\mathbf{F}}_i$

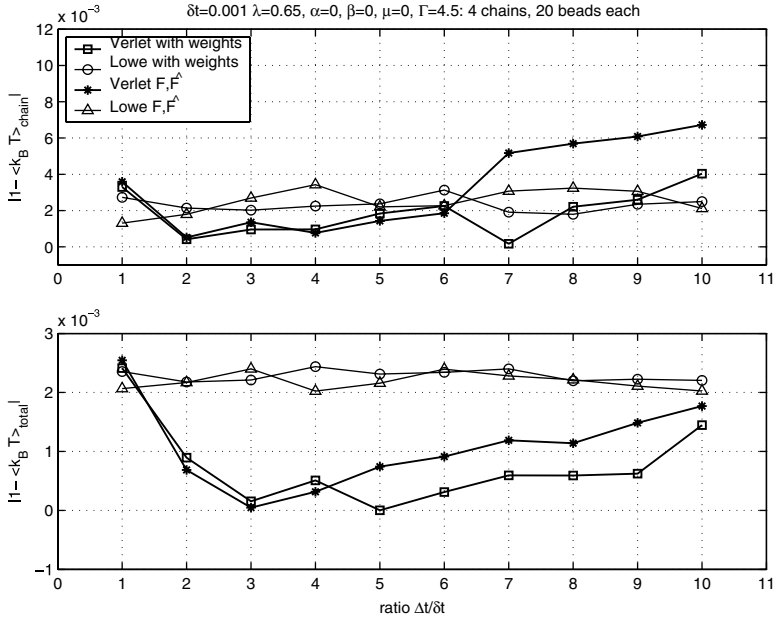

Fig. 3. Baseline case: maximum absolute error in total (upper) and chain (lower) $k_B T$ versus $\frac{\Delta t}{\delta t}$ for the vV and Lowe's methods for the *safe* range of Δt. The results also compare the non-weighted schemes with the weighted ones.

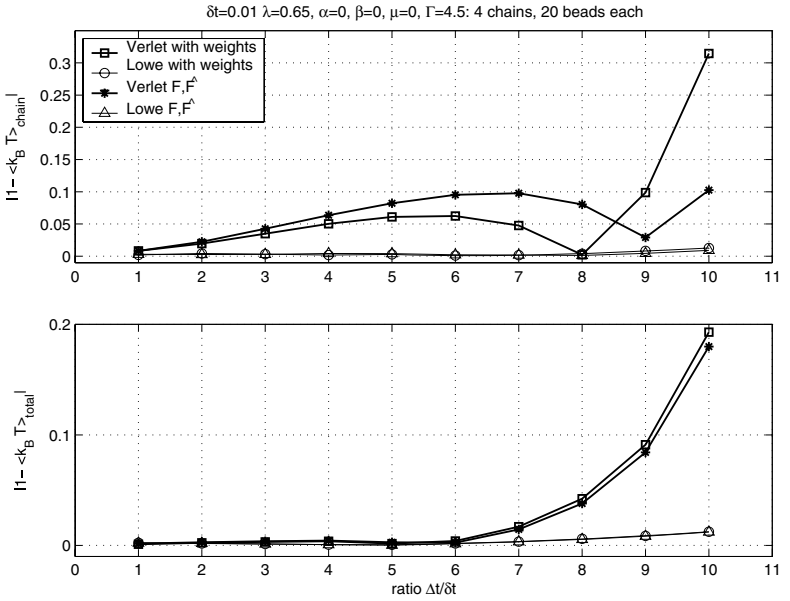

Fig. 4. Baseline case: maximum absolute error in total and chain k_BT versus $\frac{\Delta t}{\delta t}$ for the vV and Lowe's methods for the *ambitious* range of Δt. The results also compare the non-weighted schemes with the weighted ones.

However, using the proposed schemes, we will examine the maximum absolute error for the chain and total k_BT in two regimes: A *safe* one ($\Delta t \in [10^{-3}, 10^{-2}]$, $\delta t = 10^{-3}$) and a more *ambitious* one ($\Delta t \in [10^{-2}, 10^{-1}]$, $\delta t = 10^{-2}$).

5.2. The baseline case of $\mu = 0$, $\alpha = 0$, $\beta = 0$

We compare the accuracy of the vV and Lowe's schemes in Fig. 3 for the safe range, while Fig. 4 shows the maximum temperature error for large Δt. The former can be used as a guideline for the effect of the time-staggering and the error does not exceed 7×10^{-3} even for ratios of $\mathbb{K} = 10$. The latter shows realistic error values for practical applications of the proposed schemes, reaching values two orders of magnitude larger. These are precisely the errors we will attempt to minimize in the following sections. Another quantity we will monitor is the mean radius of gyration $\langle R_g \rangle$ for both schemes. Using the weighted approach, in Table 4 we show the effect of the timestep ratio on $\langle R_g \rangle$ in the ambitious range for 5-bead chains. The disagreement between the $\mathbb{K} = 1$ and the staggered values never exceeds 2% for the studied range.

5.3. Investigating other choices for μ, α and β

The relaxation parameters λ, μ, α and β of the schemes provide some flexibility in manipulating the prediction of $\hat{\mathbf{u}}$, $\hat{\mathbf{r}}_p$, $\hat{\mathbf{u}}_p$ and $\hat{\mathbf{F}}$, respectively. For simplicity the following tests will use the non-weighted time-staggering. Since the timestep dependence in Lowe's method comes from the conservative forces, we anticipate any optimal value findings to be directly applicable to the time-staggered Lowe scheme.

We attempt varying μ, α and β in the range $[-1, 1]$. By using values in the open interval $(0, 1)$ we essentially take a weighted average of the quantity between the prediction at the $(n+1)$th step and the old value at the nth step. In the limiting cases, 0 uses *only* the prediction while 1 uses *only* the nth step value. As an additional test, we also investigate negative values, thus numerically favoring the prediction up to a coefficient of 2. This disfavors the nth step value, by introducing a negative coefficient. Wider ranges are intuitively unphysical and will not be considered.

Fig. 5 shows the absolute error in k_BT for the chains and the whole system (polymer and solvent particles) for the system described earlier, i.e. a 4000-DPD fluid with four 20-bead chains governed by FENE and LJ

Table 4
$\langle R_g \rangle$ dependence on $\frac{\Delta t}{\delta t}$ for 5 beads (baseline case with $\delta t = 10^{-2}$)

$\Delta t/\delta t$	1	2	4	6	8	10
Verlet	1.0434	1.0410	1.0352	1.0311	1.0345	1.0521
σ	0.0762	0.0746	0.0730	0.0732	0.0750	0.0771
Lowe	1.0449	1.0459	1.0389	1.0435	1.0479	1.0531
σ	0.0731	0.0730	0.0741	0.0743	0.0724	0.0750

The standard deviation σ is mentioned below each case, as an indication of an error bar.

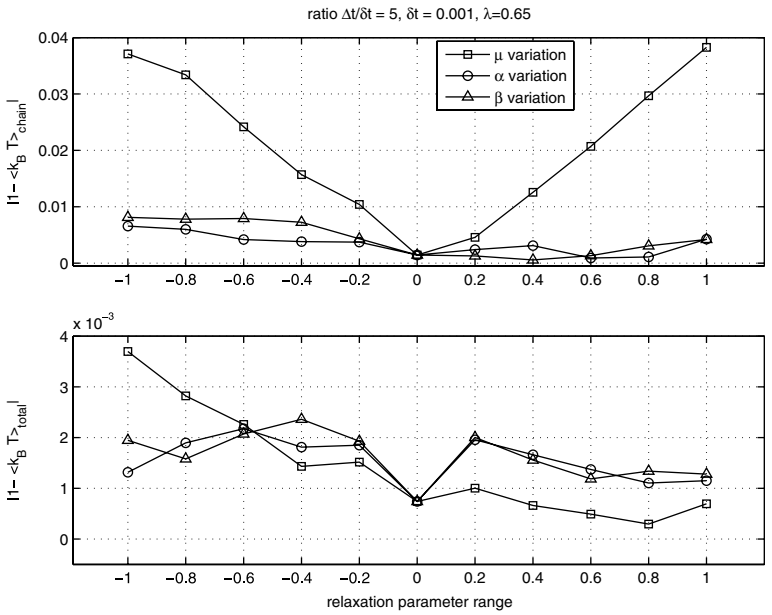

Fig. 5. Maximum absolute error in total (upper) and chain (lower) k_BT versus individual relaxation parameter variation. Optimal parameters prove to be $\mu \approx 0$, $\alpha \approx 0.6$, $\beta \approx 0.4$ when perturbed from 0, one parameter at a time.

forces. The error is plotted against the parameter range $[-1, 1]$. We note that the variation is done with *one* parameter at a time, that is, while varying one parameter, the two other parameters are fixed to 0. The ratio $\mathbb{K}$ is fixed to 5, with $\Delta t = 0.005$, $\delta t = 0.001$, rendering the timestep value safe (recall that stability for the chosen parameters requires $\delta t < 0.03$).

Accuracy in the negative parameter range proves to be worse than the positive one. Moreover, the sensitivity of the system on the variation of μ is extremely pronounced. As far as the optimal values are concerned, the three separate curves indicate that reasonable choices would be either

$$(\mu, \alpha, \beta) = (0, 0.6, 0) \quad \text{or} \quad (\mu, \alpha, \beta) = (0, 0, 0.4), \tag{6c}$$

and these will be separately investigated in the following sections. The total temperature shows an error range of $[0, 2] \times 10^{-3}$ for all positive values. Hence, error in the polymer chains *alone* will be the optimal parameter choice guideline.

Another way of investigating optimal parameter choices would be simultaneous variation of μ, α, β in the same range. Fig. 6 shows that simultaneous variation is a bad choice. Also, setting $(\mu, \alpha, \beta) = (0, 0.6, 0.4)$ simultaneously, still proved to produce an error larger than the baseline $(\mu, \alpha, \beta) = (0, 0, 0)$ case.

Equipped with the above indications, we perform the definitive investigative test in the safe range of $\Delta t \in [10^{-3}, 10^{-2}]$, $\delta t = 10^{-3}$ for the vV scheme, comparing results for the triplets $(\mu, \alpha, \beta) = (0, 0.6, 0), (0, 0, 0.4)$.

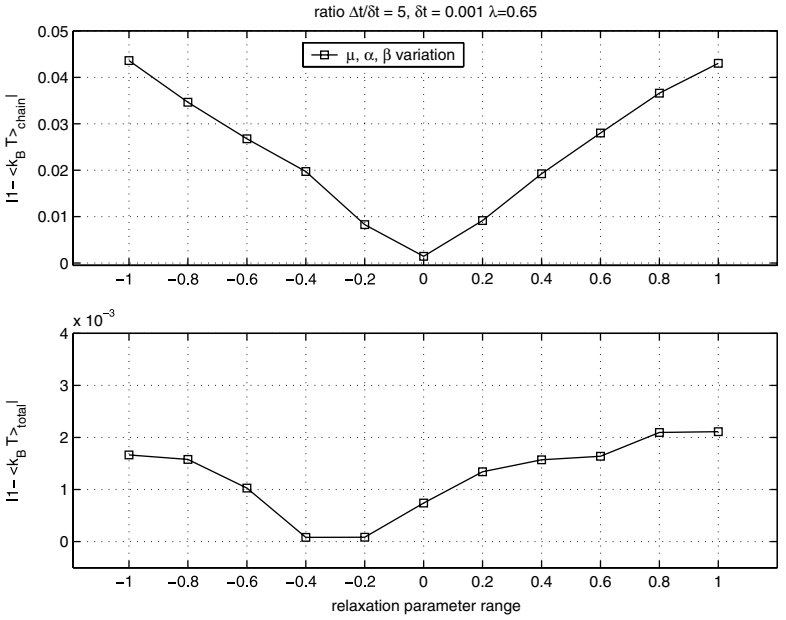

Fig. 6. Simultaneous relaxation parameter variation: a bad approach. (The quantities plotted are the same as in the previous figure.)

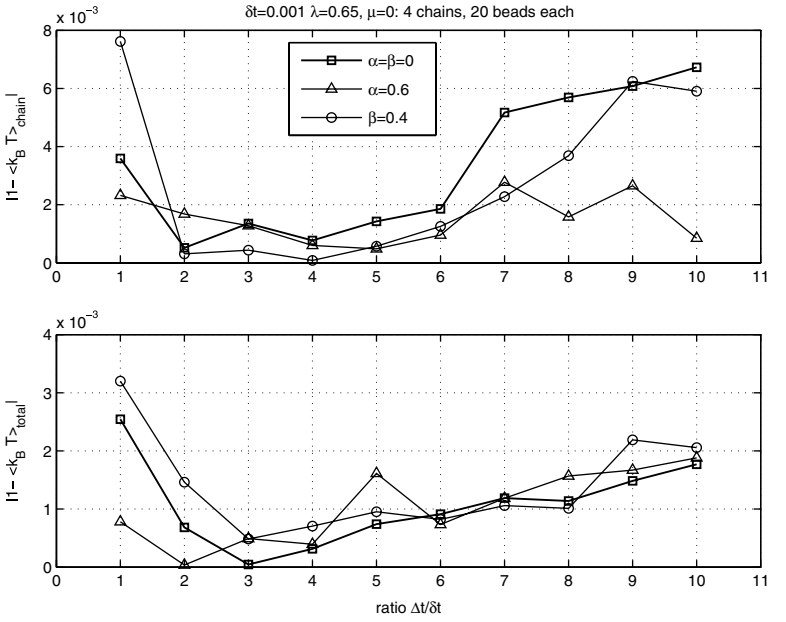

Fig. 7. Maximum absolute error in total (upper) and chain (lower) $k_{\mathrm{B}}T$ versus $\mathbb{K}$ for the optimal parameters compared to the baseline case of $\alpha = \beta = \mu = 0$. Results from the vV scheme are shown.

Summarizing the results for this section, Fig. 7 shows a mild advantage of $\beta = 0.4$ for timestep ratios $\in [2, 7]$ but $\alpha = 0.6$ performs better for ratios $\in [8, 10]$. Moreover, $\beta = 0.4$ depicts a more erratic behavior in the observed range; 1:1 ratio is favored by $\alpha = 0.6$. Both perturbations from 0 perform, in general, better than the baseline case. However, the parameter α does not appear in Lowe's method, which entails that Lowe's method can only benefit from $\beta = 0.4$. Given all of the above, we conclude that the optimal choice is

$(\mu, \alpha, \beta) = (0, 0.6, 0)$, weighted staggering: Verlet,
$(\mu, \alpha, \beta) = (0, 0, 0.4)$, weighted staggering: Lowe.

and the convergence under these parameters will be investigated in the following section for the vV and Lowe's staggered methods.

5.4. Optimal cases with weighted staggering: safe and ambitious ranges

Revisiting the safe and ambitious timestep ranges, Fig. 8 summarizes accuracy results for both methods with weighted time-staggering for the chain and total kinetic temperature in the *safe* range. It serves as a guideline on the effect of the time-staggering *alone*. Both methods prove to perform well even for ratios $\mathbb{K} = \frac{\Delta t}{\delta t} = \frac{10}{1}$. The vV scheme shows a more erratic dependence on $\mathbb{K}$ on individual polymer chains, but proves to be more accurate in this δt regime than Lowe's method as a whole (i.e., for $k_B T_{\text{total}}$).

The accuracy tests in the *ambitious* range (see Fig. 9) with the optimal parameters show a clear advantage of the proposed schemes compared to the baseline case. Even for $\mathbb{K} = 4$, vV and Lowe's methods produce an error of $\{1.9, 4.1\} \times 10^{-3}$, respectively, while the baseline case values are $\{50.3, 1.8\} \times 10^{-3}$. Clear advantage therefore is achieved in the vV case for $\mathbb{K} \in [1, 6]$ while Lowe's method shows almost the same accuracy for both the baseline and the optimal cases. Moreover, the dependence on $\mathbb{K}$ is now *monotonic*, an attractive improvement from the baseline case.

6. Computational complexity

CPU-time savings is the basic motivation for using a time-staggered scheme with two different timesteps. Fig. 10 summarizes results for four different chains in a 4000-DPD particle simulation, each having 20, 50 and 100 beads. Efficiency depends (among other factors) on how the intra-polymer pairwise interactions are handled. Since all the forces are pairwise, it is customary not to explicitly compute all the pairs in the domain, but to introduce *neighbor* (or *cell*) lists or boxes and search only in them [34]. This dramatically reduces the computational cost, which would be quadratic in N (the total number of DPD particles). Although we use a brute-force method for searching through all the pairs in a chain, an $\mathcal{O}(M^2)$ operation for M beads,

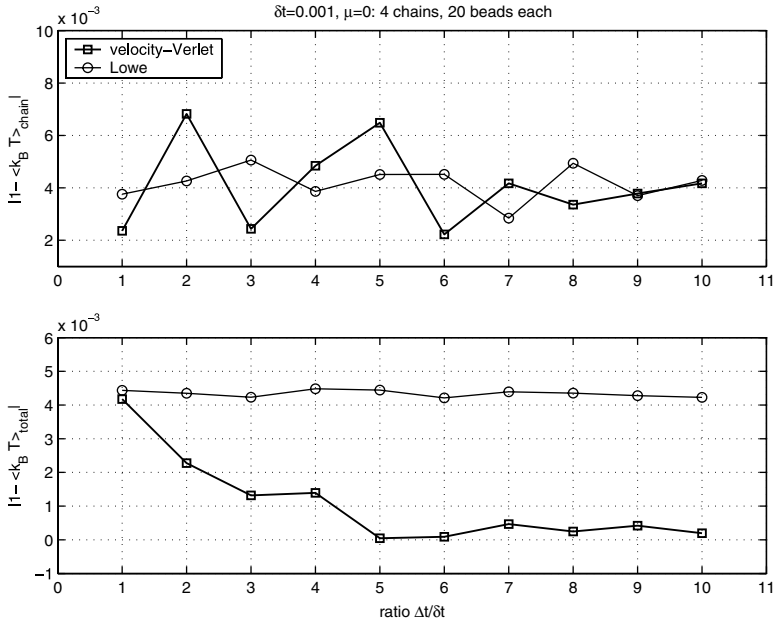

Fig. 8. Comparison of the vV ($\alpha = 0.6$) and Lowe's ($\beta = 0.4$) schemes using the optimal relaxation parameters and weighted time-staggering for the *safe* range.

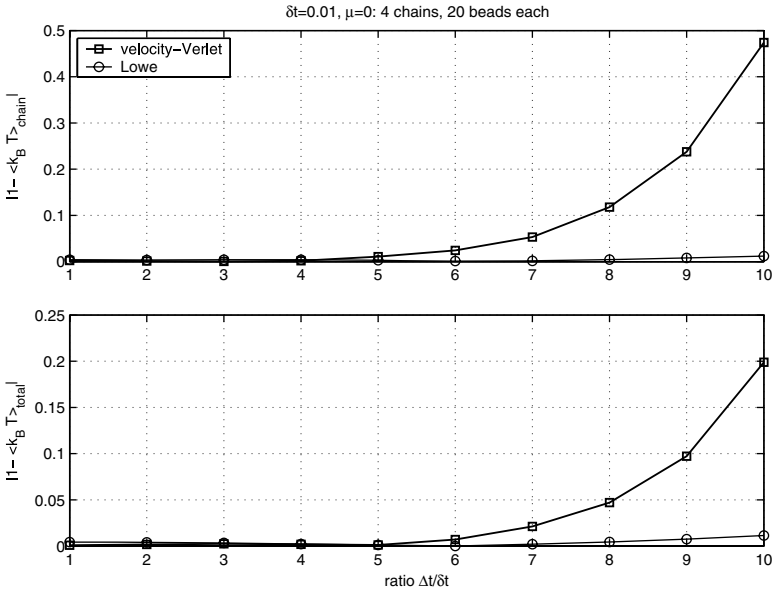

Fig. 9. Comparison of the vV ($\alpha = 0.6$) and Lowe's ($\beta = 0.4$) schemes using the optimal relaxation parameters and weighted time-staggering for the *ambitious* range.

further improvement can be achieved by using a linked-list method for the polymer chain, as is done for the solvent. This would be beneficial only for large chains. If we consider a staggered simulation of $\{\Delta t, \delta t\}$ time-steps, the speed-up of the method is defined as the ratio

$$\text{speed-up} = \frac{[\text{total CPU-time for a } \delta t \text{ simulation}]}{[\text{total CPU-time to advance to the same solution time for a hybrid staggered } \{\Delta t, \delta t\} \text{ simulation}]}.$$

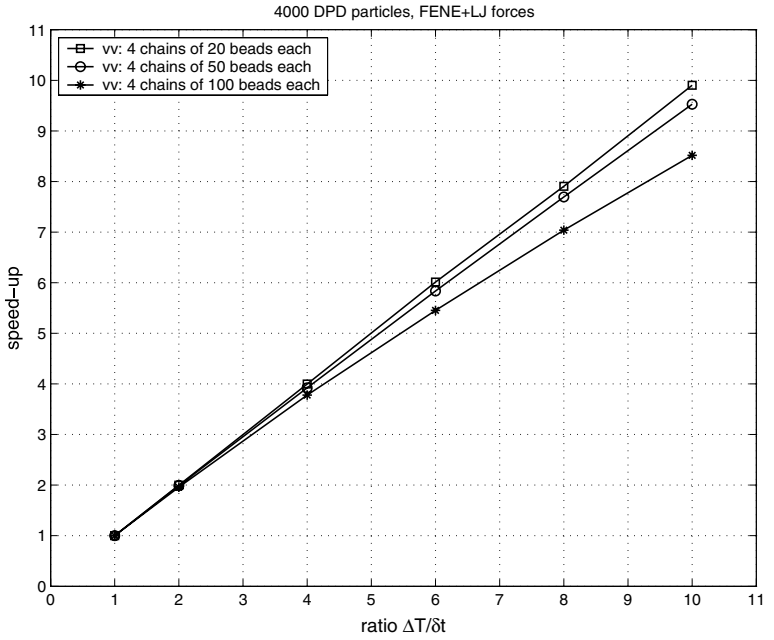

Fig. 10. Speed-up results versus $\frac{\Delta t}{\delta t}$ for the vV method for a 4000-DPD particle fluid. The polymer beads interact with each other through a FENE force and a pairwise LJ hard repulsion. The results for Lowe's method show minimal difference.

The chosen polymer force influences the speed-up, since LJ interactions require calculations of all possible pair combinations, while spring forces alone do not. Fig. 10 the speed-up for vV, while the results for Lowe's method show minimal difference. The speed-up is almost linear in dilute solutions with polymers formed by shorter chains. Larger chains show reduced (sub-linear) speed-up. In our example of brute-force pair searching for 100-bead chains, we still achieve a speed-up of 8 for $\frac{\Delta t}{\delta t} = 10$. We expect the schemes to show reduced efficiency *only* for the special case of non-dilute solutions of large polymer chains. In that case results could be further improved by introducing an extra neighbor list for bead–bead force calculations. If non-bonded interactions are present, the latter might not even be necessary.

7. The static exponent v

Since our DPD hybrid models represent, in effect, dilute polymer solutions, the dynamics of a single flexible polymer chain is of great importance for validation and physical understanding of the DPD methods. An early work by Schlijper et al. [10] has used stiff (Fraenkel) and weak (Hooke) springs, without hard LJ potentials, to map polymer-chain scaling exponents to the DPD results. Our work introduces more complex (nonlinear) forces combined with hard repulsions for various spring laws. This serves the double objective of validating the DPD simulation method as well as introducing novel combinations of interactions (such as the Fraenkel spring coupled with bead-bead repulsions).

It has been known that ideal chains are characterized by a linear relation between force and elongation, and exhibit the phenomenon of *phantom collisions*, i.e., polymeric bonds are not restricted from passing through each other. On the other hand, real chains in good solvents behave like self-avoiding walks on a lattice and do not exhibit phantom collisions. In simulations this can be achieved by introducing a repulsive force between beads i, j of the form

$$\mathbf{F}_i^{EV} = -\sum_j \frac{\partial}{\partial \mathbf{r}_i} U^{\mathrm{EV}}(\mathbf{r}_i - \mathbf{r}_j)$$

for excluded volume, given by the gradient of a potential $U^{\mathrm{EV}}(\mathbf{r}_{ij})$.

Pierre de Gennes [1] considered two critical exponents for a single chain: γ, relating to chain entropy, and v, relating to chain size. An ideal chain has a scaling law of $v = 0.5$, while a real chain with excluded volume follows the Flory formula $v = \frac{3}{d+2} = 0.6$, for three dimensions (in fact, the exponent for a self-avoiding random walk is closer to $v \approx 0.588$). DPD simulations of linear chains [10] have shown a close mapping to the 0.5 exponent, which in turn relates to the continuum Zimm model of harmonic springs [35], while some works, e.g. [36], have recovered $v \approx 0.6$ by manipulating solvent characteristics. In other words, R_{g} for ideal chains scales as

$$R_{\mathrm{g}} \propto (M-1)^{0.5},$$

while measurements of scattered light intensity versus angle verify [1] the chain size power law to be

$$R_{\mathrm{g}} \propto (M-1)^{0.6}.$$

To appreciate the practical potential of both the vV and Lowe time-staggered schemes in equilibrium we compute the static scaling law for $\mathbb{K} = \frac{\Delta t}{\delta t} = \{1, 6, 10, 20\}$ in the ambitious range $\Delta t = \{0.01, 0.06, 0.1, 0.2\}$, $\delta t = 0.01$ for the FENE and LJ with $r_{\max} = 3r_{\mathrm{c}}$. The close agreement of v depicted in Fig. 11 for this sample stiff polymeric system demonstrates the advantages in using such an algorithm: We obtain an almost linear speed-up (depending on the number of polymer chains present) in CPU-time, with negligible accuracy deviation in a timestep regime up to $\Delta t = 0.06$, i.e., three times the maximum timestep ($\Delta t \approx 0.02$) for comparable accuracy if we had used a traditional integrator.

For the vV scheme $\mathbb{K} = 20$ is not an attainable value, since the scheme is inherently dependent on the chosen timestep and $\Delta t = 0.2$ is already large, even for non-polymer, non-staggered systems. This is a "normal" deviation in accuracy due to discretization errors. Hence the maximum ratio we examine is $\mathbb{K} = 10$. For this value the observed solvent temperature is 23% higher than the set value, thus over-heating the polymer chain, rendering the radius of gyration larger. However, the static exponent still scales reasonably compared to the most accurate values of $\mathbb{K} = \{1, 6\}$. Lowe's scheme, on the other hand, shows smaller sensitivity to Δt; $\mathbb{K} = 10$

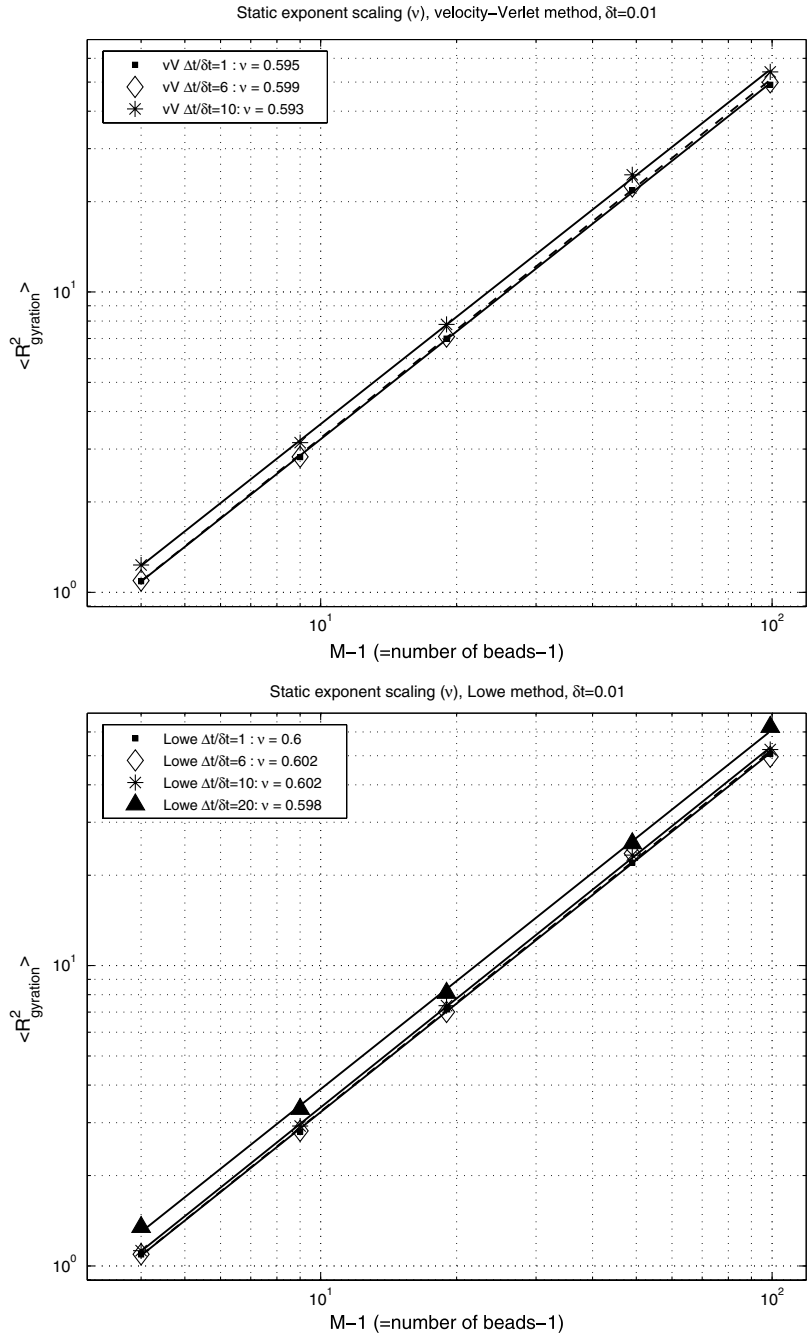

Fig. 11. The effect of time-staggering on the scaling exponent ν of the radius of gyration of a single polymer chain governed by FENE and hard LJ potentials for the vV (upper) and Lowe's (lower) scheme.

produces a $k_B T$ error $\sim$1%, but reaching $\mathbb{K} = 20$ is enough to show a significant deviation of 31% from the set temperature; similar over-heating effects on the polymer chain are observed.

8. Shear response of wormlike chains

Lowe's method provides a powerful alternative integrator to the vV scheme. The results presented in this section aim to simulate the response of λ-phage DNA molecules under steady shear, and compare the DPD

results with results from Brownian dynamics (BD) and experimental data. The wormlike chain (WLC) described in Section 3 is used for all DNA simulations for which Underhill and Doyle's [31] persistence length (λ_p) correction always applies to our results for $M > 2$. Bouchiat's [37] correction for the dumbbell case produced statistically similar results to the original Marko–Siggia (M–S) model. Since the λ_p correction studies in [31] were done with the M–S formula, we do not use Bouchiat's version.

DNA molecules under steady shear have been extensively studied in experimental [38] and computational [39,25] works. Using DPD we investigated the dynamics of a single WLC. The moving boundaries at $y = 0$, $y = L_y$ are modeled using Lees–Edwards boundary conditions [40]: particles leaving the domain at $y = 0$, L_y are advanced/retarded by an increment of $\Delta r = U_x t$, $-U_x t$, respectively, in the x-direction, where t is the time elapsed from an appropriate origin of times and U_x denotes twice the shear velocity of each boundary. Moreover, the velocity of the particle is increased/decreased by U_x, $-U_x$, accounting for both the imposed boundary condition and the velocity discontinuity between the two walls. This correction is essential, since the dissipative forces depend on the relative pairwise velocities. The rest of the boundaries are treated periodically for all the solvent DPD particles. To avoid unphysical periodicity artifacts, polymer beads *only* undergo an elastic collision in the y-direction: $(u, v, w)_{\mathrm{BEAD}} \to (u, -v, w)_{\mathrm{BEAD}}$ and $r_y \to r_y - (\Delta t) v_{\mathrm{BEAD}}$. Different chain sizes were accommodated by storing the polymer coordinates without mapping them back in the original domain. This allowed the intra-polymer forces to be calculated properly, while the collective solvent–solvent and polymer–solvent interactions were calculated with the mapped (periodic) images. The effect of the simulation box size $L_x \times L_y \times L_z$ for the presented results was investigated and proved to be negligible. For the results shown, a periodic box of dimensions $10 \times 20 \times 5$ was used in a fluid of 4000-DPD particles. The conservative force amplitude was fixed to $a_{ij} = 75 k_B T/\rho$, as in [11].

In order to properly simulate λ-phage DNA molecules under steady shear, we define the dimensionless Weissenberg number of the flow as $We = \dot{\gamma}\tau$, for a shear rate $\dot{\gamma}$. Here, τ is the polymer's longest relaxation time, which has been known to be computed by fitting an exponential analytical curve to the average mean-square extension (we note that this is *not* necessarily the end-to-end value.) This approach provides a relaxation time nearly the same (within 10%) with that obtained by fitting the late-time tail of the mean-square radius of gyration $\langle R_g^2 \rangle$.

Fig. 12 shows the fitted results. The calculated mean-square extension of an initially 30%-extended chain was fitted with $\langle x^2 \rangle = \langle x^2 \rangle_0 + x_i^2 \, e^{-t/\tau}$ to obtain the chain relaxation time τ. Here, x_i^2 is the initial stretch and $\langle x^2 \rangle_0$ is the equilibrium value. Equating the area under both curves fixed the free parameter of the fit.

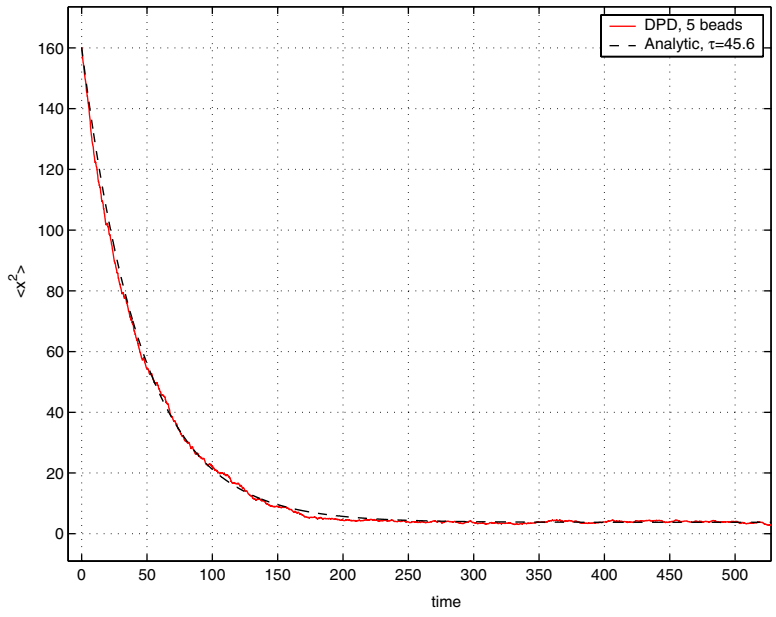

Fig. 12. Decay of the average mean-square extension $\langle x^2 \rangle$ and the corresponding exponential fit for a wormlike chain of 5 beads in a Newtonian solvent using Lowe's non-staggered method.

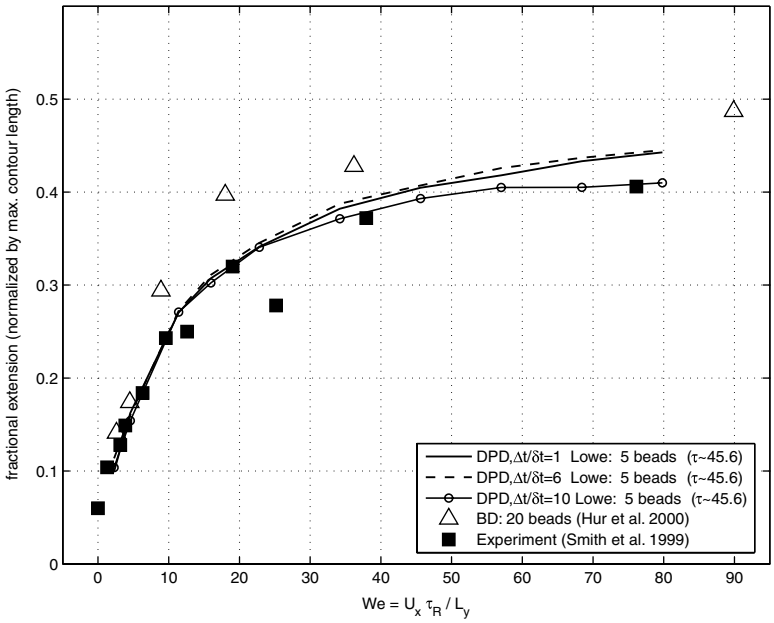

Fig. 13. Effect of $\mathbb{K} = 1, 6, 10$ under shear. Maximum projected average extension of a 5-bead DNA molecule modeled by the M–S formula versus *We*. Here, $\delta t = 0.01$.

Non-equilibrium configurations present an additional challenge on the performance of the integrating schemes. In order to demonstrate the accuracy of the proposed algorithms, we examine the effect of two different timesteps on physical quantities such as the mean maximum projected molecular extension under steady shear. Having established a satisfactory performance of Lowe's method with $\mathbb{K} = 6, 10$ in equilibrium, Fig. 13 demonstrates the performance of the method for the same timestep ratios under shear for a 5-bead WLC, and compares the results with BD [39] and experimental data [38]. The time-staggered scheme produces a slightly larger molecular extension $\langle x \rangle$ for $\mathbb{K} = 6$ with a maximum disagreement not more than 10^{-2}, an extremely attractive result for all practical purposes, given the (almost linear) CPU savings. However, $\mathbb{K} = 10$ shows some deviation of the monitored averaged quantity, with a 7% disagreement at the high Weissenberg number regimes. The limitations of the proposed schemes under shear are clear; non-equilibrium configurations impose extra constraints on the value of $\mathbb{K}$ while the errors become apparent at high shear rates.

9. Summary and discussion

Dissipative particle dynamics (DPD) is an attractive alternative to Brownian dynamics (BD) in simulating polymeric solutions. It is momentum preserving and Galilean invariant; it involves two-way coupling between the polymers and solvent, and can be used in complex-geometry domains. The computational cost scales linearly with the number of particles if the DPD algorithm is properly implemented, hence very large systems can be simulated on serial computers. The use of hard potentials, however, to describe the microscopic dynamics of the polymers limits substantially the timestep in integrating the stochastic differential equations of motion. Specifically, the typical timestep in polymer systems using the standard available algorithms is about 20 times smaller than the timestep employed in single-phase simulations. The time-staggered algorithms proposed in the current work relax this constraint as they allow greater timesteps, i.e., by about a factor of 10 for the velocity-Verlet algorithm and by a factor of 20 for Lowe's method.

Specifically, we have developed parametric *families* of time-staggered schemes for integrating the DPD equations by introducing several relaxation parameters, and sought to determine their best values via equilibrium simulations of dilute polymer solutions. These relaxation parameters allow enhanced accuracy in the numerical solutions without the need of re-evaluating the hydrodynamic forces many times which would

increase the computational cost in an unfavorable way. This approach was successfully implemented for single-phase DPD simulations by Warren and Groot [11] and motivated the current work. The time scale separation introduced by the soft potential for the solvent and the hard potential for the polymers allows the effective use of a subsycling, in a spirit similar to macroscale CFD in advection–diffusion systems where advection may be advanced with small timesteps with explicit integrators whereas diffusion is typically advanced with larger timesteps via implicit time-integrators.

The velocity-Verlet (vV) algorithm we considered here integrates the standard DPD equations that involve conservative, dissipative and random forces. Lowe's alternative method, on the other hand, involves only conservative forces and achieves thermodynamic equilibrium by re-equilibration of all the particle velocities through a Maxwell distribution. Lowe's method is faster than the vV algorithm, and as we have demonstrated herein, it uses almost twice as large timesteps compared to vV for comparable accuracy. Another important advantage of Lowe's method relates to the value of Schmidt number, Sc, which can be controlled through the parameter Γ (see Table 2). Lowe [15] has argued that $Sc \propto \Gamma^2$, and this has been verified via systematic DPD simulations in [41]; for typical liquids the value of Schmidt number is about 1000. In the vV algorithm the value of Schmidt number is around one for $k_B T = 1$, see [11,41]. We note, however, that in time-staggered algorithms the value of the parameter Γ should be kept the same as in the standard time-integrators in order to achieve the same value of Schmidt number in both cases. This is because the diffusion coefficient scales as $1/\Gamma$ and it is approximately independent of the size of the timestep despite the fact that the product $\Gamma \times \Delta t$ controls the thermalization process in Lowe's method [41].

Acknowledgments

The authors thank the referees for their comments and for suggesting useful references. This research is funded by NSF under the IMAG program for multi-scale modeling.

References

[1] P.-G. de Gennes, Scaling Concepts in Polymer Physics, Cornell University Press, Ithaca, NY, 1979.
[2] P. Ahlrichs, B. Dünweg, Simulation of a single polymer chain in solution by combining Boltzmann and molecular dynamics, J. Chem. Phys. 111 (17) (1999) 8225–8239.
[3] A. Malevanets, R. Kapral, Mesoscopic model for solvent dynamics, J. Chem. Phys. 110 (17) (1999) 8605.
[4] A. Malevanets, R. Kapral, Solute molecular dynamics in a mesoscale solvent, J. Chem. Phys. 112 (16) (2000) 7260.
[5] A. Malevanets, J. Yeomans, Dynamics of short polymer chains in solution, Europhys. Lett. 52 (2000) 231.
[6] E. Falck, O. Punkkinen, I. Vattulainen, T. Ala-Nissila, Dynamics and scaling of two-dimensional polymers in a dilute solution, Phys. Rev. E 68 (2003) 050102.
[7] H. Noguchi, G. Gompper, Fluid vesicles with viscous membranes in shear flow, Phys. Rev. Lett. 93 (2004) 258102.
[8] P.J. Hoogerbrugge, J.M. Koelman, Simulating microscopic hydrodynamic phenomena with dissipative particle dynamics, Europhys. Lett. 19 (3) (1992) 155–160.
[9] P. Español, P. Warren, Statistical mechanics of dissipative particle dynamics, Europhys. Lett. 30 (4) (1995) 191–196.
[10] A. Schlijper, P. Hoogerbrugge, C. Manke, Computer simulation of dilute polymer solutions with the dissipative particle dynamics method, J. Rheol. 39 (3) (1995) 567.
[11] R.D. Groot, P.B. Warren, Dissipative particle dynamics: bridging the gap between atomistic and mesoscopic simulation, J. Chem. Phys. 107 (11) (1997) 4423–4435.
[12] C. Pierleoni, J.-P. Ryckaert, Molecular dynamics investigation of dynamic scaling for dilute polymer solutions in good solvent conditions, J. Chem. Phys. 96 (11) (1992) 8539–8551.
[13] I. Pagonabarraga, M.H.J. Hagen, D. Frenkel, Self-consistent dissipative particle dynamics algorithm, Europhys. Lett. 42 (1998) 377.
[14] W. den Otter, J. Clarke, The temperature in dissipative particle dynamics, Europhys. Lett. 53 (2001) 426–431.
[15] C.P. Lowe, An alternative approach to dissipative particle dynamics, Europhys. Lett. 47 (2) (1999) 145–151.
[16] T. Shardlow, Splitting for dissipative particle dynamics, SIAM J. Sci. Comput. 24 (4) (2003) 1267–1282.
[17] E. Peters, Elimination of time step effects in DPD, Europhys. Lett. 66 (3) (2004) 311–317.
[18] G. Besold, I. Vattulainen, M. Karttunen, J. Polson, Towards better integrators for dissipative particle dynamics simulations, Phys. Rev. E 62 (6) (2000) R7611.
[19] P. Nikunen, M. Karttunen, I. Vattulainen, How would you integrate the equations of motion in dissipative particle dynamic simulations? Comput. Phys. Commun. 153 (2003) 407–423.
[20] G.E. Karniadakis, S.J. Sherwin, Spectral/hp Element Methods for Computational Fluid Dynamics, second ed., Oxford University Press, Oxford, 2005.

[21] T. Bishop, R.D. Skeel, K. Schulten, Difficulties with multiple timestepping and the fast multipole algorithm in molecular dynamics, J. Comput. Chem. 18 (14) (1997) 1785–1791.
[22] L. Verlet, Computer 'experiments' on classical fluids. I: Thermodynamical properties of Lennard-Jones molecules, Phys. Rev. 159 (1967) 98–103.
[23] A. Jakobsen, O. Mouritsen, G. Besold, Artifacts in dynamical simulations of coarse-grained model lipid bilayers, J. Chem. Phys. 122 (2005) 204901.
[24] B.M. Forrest, U.W. Suter, Accelerated equilibration of polymer melts by time-coarse-graining, J. Chem. Phys. 102 (18) (1995) 7256–7266.
[25] R.M. Jendrejack, J.J. de Pablo, M.D. Graham, Stochastic simulations of DNA in flow: dynamics and the effects of hydrodynamic interactions, J. Chem. Phys. 116 (2002) 7752–7759.
[26] O. Kratky, G. Porod, Röntgenuntersuchung gelöster fadenmoleküle, Rec. Trav. Chim. 68 (1949) 1106–1115.
[27] H. Yamakawa, Modern Theory of Polymer Solutions, Harper and Row, New York, 1971.
[28] S.F. Sun, Physical Chemistry of Macromolecules, Wiley, New York, 1994.
[29] J.F. Marko, E.D. Siggia, Stretching DNA, Macromolecules 28 (1995) 8759–8770.
[30] R.G. Larson, T.T. Perkins, D.E. Smith, S. Chu, Hydrodynamics of a DNA molecule in a flow field, Phys. Rev. E 55 (2) (1997) 1794–1797.
[31] P.T. Underhill, P.S. Doyle, On the coarse-graining of polymers into bead-spring chains, J. Non-Newtonian Fluid Mech. 122 (1) (2004) 3–31.
[32] H.C. Andersen, Molecular dynamics simulations at constant pressure and/or temperature, J. Chem. Phys. 72 (4) (1980) 2384–2396.
[33] Q. Ma, J.A. Izaguirre, R.D. Skeel, Verlet-I/R-RESPA/Impulse is limited by nonlinear instabilities, SIAM J. Sci. Comput. 24 (6) (2003) 1951–1973.
[34] M.P. Allen, D.J. Tildesley, Computer Simulation of Liquids, Oxford University Press, Oxford, 1989.
[35] R.G. Larson, The Structure and Rheology of Complex Fluids, Oxford University Press, Oxford, 1999.
[36] Y. Kong, C.W. Manke, W.G. Maddenand, A.G. Schlijper, Effect of solvent quality on the conformation and relaxation of polymers via dissipative particle dynamics, J. Chem. Phys. 107 (2) (1997) 592–602.
[37] C. Bouchiat, M.D. Wang, J.-F. Allemand, T. Strick, S.M. Block, V. Croquette, Estimating the persistence length of a worm-like-chain molecule from force-extension measurements, Biophys. J. 76 (1999) 409–413.
[38] D.E. Smith, H.P. Babcock, S. Chu, Single polymer dynamics in steady shear flow, Science 283 (1999) 1724.
[39] J.S. Hur, E.S.G. Shaqfeh, R.G. Larson, Brownian dynamics simulations of single DNA molecules in shear flow, J. Rheol. 44 (4) (2000) 713–742.
[40] A.W. Lees, S.F. Edwards, The computer study of transport processes under extreme conditions, J. Phys. C 5 (1972) 1921.
[41] V. Symeonidis, Numerical methods for multi-scale modeling of non-Newtonian flows, Ph.D. Thesis, Brown University, 2006.